AD NUMBER

AD880478

LIMITATION CHANGES

TO:

Approved for public release; distribution is unlimited. Document partially illegible.

FROM:

Distribution: Further dissemination only as directed by Advanced Research Projects Agency, Attn: TIO, 1400 Wilson Blvd., Arlington, VA 22209, JAN 1971, or higher DoD authority. Document partially illegible.

AUTHORITY

USAMC ltr, 24 Jun 1971

REPORT NO. 1

MELT-GROWN OXIDE-METAL COMPOSITES

SEMI-ANNUAL TECHNICAL REPORT

(Period: 1 July 1970 to 31 December 1970)

Project Director
A. T. Chapman

Sponsored By
Advanced Research Projects Agency
Department of Defense
ARPA ORDER NO. 1637

Contract No. DAAHO1-70-C-1157

January 1971

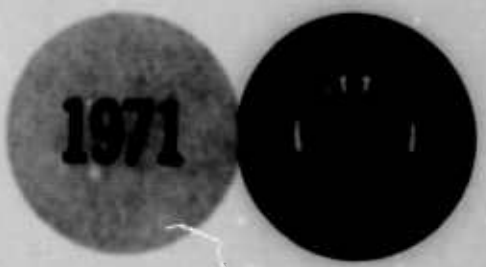

School of Ceramic Engineering
GEORGIA INSTITUTE OF TECHNOLOGY
Atlanta, Georgia

DISCLAIMER NOTICE

THIS DOCUMENT IS THE BEST QUALITY AVAILABLE.

COPY FURNISHED CONTAINED A SIGNIFICANT NUMBER OF PAGES WHICH DO NOT REPRODUCE LEGIBLY.

Report No. 1

MELT-GROWN OXIDE-METAL COMPOSITES

SEMI-ANNUAL TECHNICAL REPORT

(Period: 1 July 1970 - 31 December 1970)

From

THE SCHOOL OF CERAMIC ENGINEERING

GEORGIA INSTITUTE OF TECHNOLOGY

ATLANTA, GEORGIA 30332

PROJECT DIRECTOR: A. T. CHAPMAN

January 1971

SPONSORED BY

ADVANCED RESEARCH PROJECTS AGENCY

DEPARTMENT OF DEFENSE

ARPA ORDER NO. 1637

CONTRACT NO. DAAHOI-70-C-1157

PERSONNEL PARTICIPATING IN PROJECT

Principal Investigators

J. F. Benzel

R. K. Feeney

R. J. Curtis

J. W. Hooper

Graduate Students

N. E. Grynkewich

C. C. Jen

T. A. Johnson

Y. S. T. Lin

J. Pepper

G. T. Tucker

M. D. Watson

TABLE OF CONTENTS

Section	Title	Page
I	INTRODUCTION	1
II	UNIDIRECTIONAL SOLIDIFICATION BEHAVIOR OF OXIDE-METAL SYSTEMS	6
III	STRUCTURAL AND CHEMICAL CHARACTERIZATION OF OXIDE-METAL COMPOSITES	16
	A. Characterization Program	17
	B. Experimental Results	18
IV	THEORETICAL ANALYSIS OF ELECTRON EMITTING ARRAYS	28
V	FORMATION OF OPTIMUM EMITTING ARRAYS	35
	A. Composite Growth Equipment	35
	B. Analysis of Oxide-Metal Solidification	38
	C. Chemical Etching Procedure	47
VI	ELECTRON EMISSION MEASUREMENTS	50
	A. Experimental Facility	50
	B. Preliminary Field Emission Results	52
VII	SUMMARY	55

LIST OF ILLUSTRATIONS

Figure	Title	Page
1	Scanning Electron Micrograph of UO_2-W Composite Displaying Uniform W Fiber Distribution.	19
2	Scanning Electron Micrograph of UO_2-W Composite Displaying Circular Primary Phase Areas of UO_2 Plus Eutectic Growth.	19
3	Scanning Electron Micrograph of Sharpened Tungsten Fiber Tips After Chemical Etching.	22
4	Transmission Electron Micrograph of UO_2-W Composite Showing Hexagonal Cross Section of Several W Fibers.	23
5	Scanning Electron Micrograph of Single W Fiber Chemical Etch Has Altered Octagonal Cross Section at Fiber Base to a Square Shape at the Tip.	24
6	High Voltage Transmission Electron Micrograph of Tungsten Fiber in UO_2 Matrix After Sample Thinning by Ion Etching. Fiber is Viewed at Approximately 45° Off Fiber Axis.	26
7	Dependence of Current Density on Electric Field, for various Values of $\sigma r^2/s^2$).	32
8	Dependence of Current Density on Voltage, for Various Values of s.	33
9	Schematic Diagram of Facility for the Growth of Oxide-Metal Composites.	36
10	Proposed Phase Diagram for the System UO_2-W.	39

LIST OF ILLUSTRATIONS (Cont.)

Figure	Title	Page
11	Scanning Electron Micrographs of UO_2-W Composites Showing Influence of Oxide-Metal Ratio and Growth Rate on the Composite Structure and W Fiber Diameter and Density. Samples Chemically Etched to Expose the Fibers.	
11a	Near Eutectic Composition. Slow Growth Rate.	41
11b	Near Eutectic Composition. Fast Growth Rate.	41
11c	Oxide-Rich Composition. Slow Growth Rate.	42
11d	Oxide-Rich Composition. Fast Growth Rate.	42
12	Scanning Electron Micrograph of Oxide-Rich UO_2-W Structure Showing W "Halo" Partially Encircling Primary Phase Areas of UO_2.	46
13	Overall View of Electron Emission Test Facility and Associated Vacuum Equipment.	51
14	Assembled Diode Structure for Emission Testing.	53

FORWORD

This Research was sponsored by the ADVANCED RESEARCH PROJECTS AGENCY of the DEPARTMENT OF DEFENSE under ARPA ORDER NO. 1637 and was monitored by the US ARMY MISSILE COMMAND under Contract No. DAAHOI-70-C-1157.

Views and conclusions expressed herein are the primary responsibility of the author or the contractor and should not be interpreted as representing the official opinion or policy of USAMICOM, ARPA, DOD or any other agency of the Government.

ABSTRACT

Research was initiated to understand and control the parameters leading to the successful growth of oxide-metal composites and to evaluate the electron emission performance of these structures. Numerous oxides, binary oxide compounds and oxide mixtures have been tested to determine their suitability for induction melting using an rf frequency of 27 mhz. Procedures employing scanning electron microscopy and x-ray diffraction have been developed to characterize oxide-metal composite samples. Metallic fiber morphology has been related to growth direction. A theoretical analysis of expected electron field emission from the array of metallic pins formed during composite growth has been performed using pin diameter, pin spacing, applied voltage and interelectrode spacing as variables. A preliminary description of the solidification behavior of oxide-metal systems is proposed, based on a tentative phase diagram, different oxide-metal ratios and variable growth rates. A diode assembly for field emission testing has been constructed, and the initial field emission testing of an oxide-metal composite sample is described.

SECTION I

INTRODUCTION

This is the initial report for the "Melt-Grown Oxide-Metal Composite" research project, ARPA Order No. 1637, and it covers the contract period 1 July 1970 through 31 December 1970. The techniques used to grow this unique class of materials containing many millions of less than 1 μ diameter tungsten fibers per square centimeter, uniformly distributed in a refractory oxide matrix, will be briefly reviewed to provide background information for interpreting this and subsequent reports. The major research objectives of the various areas of this project are also outlined.

A modified floating-zone technique has been used to grow single crystals of refractory oxides and is employed to grow the oxide-metal composites. In this technique pressed rods of the oxide-metal mixture are sintered inside rf heated molybdenum tubes in an inert atmosphere to densify and preheat the material. (A typical growth arrangement is shown schematically in Figure 9 of this report.) After the initial heating, which also serves to increase the electrical conductivity of the oxides, the molybdenum tube heaters are separated to expose approximately 2 cm

of the rod to an rf field of 3 to 30 megahertz, depending on the material to be melted. The concurrent increase of temperature, electrical conductivity, and resistance heating continues until the interior of the rod melts at temperatures up to 3000°C. The high radiant heat loss from the surface and the inherent low thermal conductivity of the oxides maintains the skin of the rod well below the eutectic temperature of the mixture. Composite growth is obtained by moving the molten zone up through the rod. In practice a cavity is generated in the molten zone because of the difference in density between the initial polycrystalline rod and solidified composite. During growth, the oxide and metal melts from the roof of this cavity and solidifies at the base.

During the growth of pure oxides it was found advantageous to rotate the rods at speeds above 300rpm. During rotation the molten material is centrifugally cast against the sides of the cavity; thus, the liquid-solid interface is modified so that crystallization in the center of the rod leads solidification near the circumference of the rod and promotes the uniform growth of one crystallographic orientation across the entire melted zone. The need for rotation during the growth of oxide-metal composites is unresolved at present because similar structures have been successfully obtained both with and without rotation. The occurrence of cell or grain boundaries across the composite structure may minimize the need for the liquid-solid interface geometry produced by rotation. To date ordered oxide-metal structures have been achieved in the systems UO_2-W, stabilized

ZrO_2-W, and $(U,Th)O_2$-W.

The primary technical objective of this project is to understand the solidification processes leading to coupled growth and ordered microstructures after melting oxide-metal mixtures, and to successfully produce useable samples of these composites and evaluate their use for practical applications. The potential use of these composites for electron emitters is being investigated first because structures containing between 4 and 25 million exposed W fibers per square centimeter can easily be attained. The research program is divided into five areas to meet these objectives.

A. UNIDIRECTIONAL SOLIDIFICATION BEHAVIOR OF OXIDE-METAL SYSTEMS

A study of the chemical, thermal, and mechanical variables active during solidification of numerous oxides and oxide-metal systems is in progress to understand the parameters which control successful oxide-metal composite growth. Analysis of solidification in systems which do not yield ordered eutectic structures may prove equally as valuable as studies of systems which readily achieve ordered structures.

B. STRUCTURAL AND CHEMICAL CHARACTERIZATION OF OXIDE-METAL COMPOSITES

The composite growth morphology, orientation relationships and composition profiles are being studied using predominantly

x-ray diffraction and scanning electron microscopy techniques. This information will be combined with the solidification studies to establish the parameters controlling oxide-metal solidification behavior.

C. THEORETICAL ANALYSIS OF ELECTRON EMITTING ARRAYS

Current mathematical descriptions of the electron emission from point sources are being used to calculate optimum fiber geometries for field and thermionic emission from the oxide-metal composites. These studies will be correlated with the experimental emission measurements to help interpret the actual emitter behavior.

D. FORMATION OF OPTIMUM EMITTING ARRAYS

Experiments are in progress in model oxide-metal systems which readily form ordered structures (e.g. W with UO_2 and ZrO_2) to establish the influence that controllable growth parameters exert on the microstructure. Future growth studies will be designed to alter existing oxide-metal geometries toward structures which the theoretical analysis shows will yield optimum emitting performance. Chemical and electrolytic etching are being tested as techniques to shape the W pins for enhanced field emission.

E. ELECTRON EMISSION MEASUREMENTS

Suitably prepared composites are being tested as diodes to evaluate their use as field emitters. Thermionic testing is planned in the future. The emission performance is being studied as a function of array geometry, and the electrical variables of field strength, interelectrode spacing, and current density. These studies will establish the potential of oxide-metal composites for use as electron emitters.

Other applications where these composites could probably be used include electro-optic devices and in microcircuit structures. These topics will be reviewed to find specific areas where the oxide-metal structures would offer definite advantages over present technology.

SECTION II

UNIDIRECTIONAL SOLIDIFICATION BEHAVIOR OF OXIDE-METAL SYSTEMS

Melting and subsequent controlled solidification of refractory oxides and oxide-metal mixtures have been previously accomplished[1,2,3,4] using high (4 to 30mhz) frequency rf heating. This technique is limited to systems that have sufficient electrical conductivity at elevated temperatures to support eddy-current heating at the level required to produce internal melting. During the first half of this contract period a number of oxides, binary oxide compounds and oxide mixtures have been tested to determine their suitability for internal melting using the rf coupling scheme.

All of the materials studied were made into 3/4 inch diameter pellets by pressing -325 mesh powders in a two punch steel die at about 2500 psi. These prepressed cylinders were then placed in an evacuated rubber envelope and hydrostatically pressed to 50,000 psi to increase their density. Final pellet height varied from 1/2 to 1 1/2 inches.

Before an attempt was made to rf couple to any pellet, it was either sintered in a ceramic processing furnace or in a one inch diameter inductively heated SiC cylinder. The

sintered test pellets were placed inside SiC tubes which preheated the pellets to temperatures between 1000 and 1670°C and increased their electrical conductivity prior to the rf coupling test. The SiC tube was located inside the work coil of a 27 mhz rf generator which, after preheating, allowed the melting behavior of these materials to be tested by simply removing the hot SiC preheater and exposing the test pellets to the rf field.

EXPERIMENTAL RESULTS

A compilation of the test results including preheat temperatures, rf coupling, and melting behavior and miscellaneous comments for the three classes of materials - oxides, oxide compounds and oxide mixtures - are presented in Tables I, II, and III respectively.

Of the single oxides tested (Table I), only CeO_2 formed a stable molten zone. Cr_2O_3, TiO_2 and NiO might also be successfully melted if their stoichiometry problem can be overcome. If the electrical conductivity of Al_2O_3, MgO and Y_2O_3 can be increased by higher preheating, increased density, or doping with impurities, these materials are also candidates for internal melting by induction heating. The use of a higher frequency rf field may also increase the chances of melting Pr_2O_3.

TABLE I

INDUCTION MELTING BEHAVIOR OF SINGLE OXIDES AT 27 MHz.

Oxide	Preheating °C	Behavior rf Coupled	Melted	Comments or Problems
Al_2O_3	1600	No	No	-
CaO	1300	Yes	No	Sublimed
CeO_2	1425	Yes	Yes	Molten area turned blue indicating reduction of the oxygen cerium ratio.
Cr_2O_3	1670	Yes	Yes	Stoichiometry change occurred. Cr metal observed in polished specimen.
MgO	1600	No	No	-
NiO	1250	Yes	Yes	Surface of pellet melted, sample was reduced, Ni metal observed in polished specimen.
Pr_2O_3	1275	Yes[1]	Yes	Only very small area melted, sample cracked on cooling.
SrO	1550	No	No	-
TiO_2	1580	Yes[1]	Yes	Molten zone melted through to surface and released liquid, some reduction observed in molten zone.
WO_3	1300	Yes	Yes	Liquid released through cracks, areas of different oxidation states present

Table I Continued

Oxide	Preheating °C	Behavior rf Coupled	Melted	Comments or Problems
Y_2O_3	1600	Slightly	No	-
ZnO	1400	Yes	?	Sublimed

(1) A 9 mhz induction generator was used instead of the usual 27 mhz generator.

TABLE II

INDUCTION MELTING BEHAVIOR OF BINARY OXIDE COMPOUNDS AT 27 Mc.

Oxide Compound	Preheating °C	Behavior rf Coupled	Melted	Comments or Problems
Al_4CaO_7	1560	Very Slightly	No	Cracked on cooling
Al_2MgO_4	1650	No	No	Spinel
$Al_4Mg_2Si_5O_{18}$	1500	No	No	Cordierite
Al_2TiO_5	1650	No	No	-
$BaFe_2O_4$	1010	No	No	Cracked badly on cooling.
$BaFe_{12}O_{19}$	1250	Yes	Yes	Molten material ejected through cracks.
$BaNiO_2$	1150	Yes	?	Nickel metal coating formed just below sample surface.
$BaO \cdot Fe_2O_3$	1150	-	-	Melted during preheat, resulting solid very brittle.
$BaSnO_3$	1150	No	No	Cracked badly during firing.
$BaTiO_3$	1530	Yes[1]	No	Must be preheated very slowly to prevent cracking.
$BaZrO_3$	1400	No	No	-
$Cr_2Y_2O_6$	1610	Yes	No	-
Fe_2TiO_5	1360	Yes	Yes	Cracked during preheating.

Table II Continued

Oxide Compound	Processing °C	Sintering at Pressure	Heated	Comments or Reactions
$CePTiO_3$	1150	No	No	*
$CePTiO_4$	1550	No	No	*

(*) A 5 kJ/J combustion generator was used instead of the usual CT gas generator.

TABLE III

EXOTHERMIC MELTING REACTION OF OXIDE MIXTURES AT 27 MM.

Oxide Mixture	Preheating °C	Behavior at Melting	Behavior Melted	Comments or Products
Al_2O_3 + TiO_2	1750	No	No	Pellet is [illegible] during cooling.
Al_2O_3 + ZrO_2	1800	No	No	Powder during cooling.
Al_2O_3 + ThO_2	1750	No	No	Fritted in N_2 atmosphere. Loose on cooling.
Al_2O_3 + Cr_2O_3	1500	No	No	"
Al_2O_3 + MnO_2	1450	No	No	"
Al_2O_3 + Fe_2O_3	1650	No	No	"
Al_2O_3 + Co_2O_3	1550	No	No	"
Al_2O_3 + NiO	1600	No	No	"
Al_2O_3 + Cu_2O	1650	No	No	"
Al_2O_3 + ZnO	1700	No	No	"
MgO + ZrO_2	1850	Yes	No	MgO fumes partially evolved.
MgO + ThO_2	1850	Yes	No	Same as ZrO_2.
ZrO_2 + ThO_2	1800	Yes	No	Incandescence established at 1800°C.

Table III Continued

Oxide Mixture	Preheating °C	Behavior rf Coupled	Melted	Comments or Problems
NiO + 80% MgO	1600	Yes	No	Same as 60% MgO.
ZnO + 10% Al_2O_3	1400	Yes	Yes	Sublimed, melted zone very porous.
ZnO + 30% Zr_2O_3	1400	Yes	Yes	Liquid expelled through walls of pellet.
ZnO + 20% TiO_3	1450	Yes	Yes	Interior became molten in only isolated areas and liquid was expelled through walls of pellet.
ZrO_2 + 5% CaO	1580	Yes	Yes	Stable internal molten zone.
ZrO_2 + 10% Y_2O_3	1600	Yes	Yes	Stable internal molten zone established after 3 minute exposure to rf field.
ZrO_2 + 15% Y_2O_3	1600	Yes	Yes	Stable internal molten zone.

Of the oxide compounds tested, Table II, iron titanate appeared to be the best candidate for rf melting if the cracking problem can be controlled by slower preheating. $BaTiO_3$ and $Cr_2Y_2O_6$ are also attractive materials for further testing, using a higher frequency field for the $BaTiO_3$ and a higher preheat temperature for the $Cr_2Y_2O_6$.

The stabilized zirconia mixtures described in Table III all formed stable internal molten zones when subjected to a 27 mhz field. If the high MgO compositions of the NiO-MgO solid solution series were preheated to a higher temperature, they also might be good candidates for internal melting. ZnO readily coupled to the rf field but sublimed badly prior to melting (see Table I). The three ZnO mixtures shown in Table III were an attempt to create a stable eutectic melt below the sublimation point of ZnO. These attempts were only partially successful.

The preceding tables indicated there were four principle reasons why stable internal molten zones were not achieved in the materials tested. These are:

(1) The efficiency of induction coupling was too low to provide the power necessary to achieve an internal molten zone.

(2) The surface of sample pellets did not emit enough thermal energy to remain solid and contain the molten zone.

(3) The specimens broke up due to thermal stresses, and

(4) The starting materials were unstable because of sublimation or stoichiometry changes.

There are a number of approaches which may be used to improve the chances of successful induction melting oxide materials. Improved coupling efficiency can be obtained with higher rf frequencies, closer sample coil geometries, and increased rf power. Higher preheat temperatures, impurity doping, and stoichiometry control can be utilized to increase the electrical conductivity of the oxides. Further work with the oxides is in progress to exploit the above possibilities for increasing electrical conductivity. Glassy carbon preheat tubes have been received and will be used to increase the preheat temperatures of those materials that appeared close to coupling at lower temperatures.

SECTION III

STRUCTURAL AND CHEMICAL CHARACTERIZATION OF OXIDE-METAL COMPOSITES

Scanning electron microscopy (SEM), non-dispersive x-ray analysis and various x-ray diffraction techniques were selected as suitable methods for the characterization of melt-grown oxide-metal composites. A program was devised which will ensure a comprehensive and efficient characterization of composite specimens using these three techniques. Aspects of this program which were covered in this report period included an evaluation of the backscattered and secondary emission mode of operation in the SEM, an analysis of the information obtainable from scanning electron stereomicrographs, an SEM study of metal fiber growth forms in selected samples, the development of procedures for x-ray orientation studies, and the determination of some initial orientation relationships and lattice parameters using x-ray techniques. In addition, various pieces of equipment, notably a new oscilloscope camera for the SEM and a doubly bent graphite monochromator for the x-ray diffractometer, were installed. These items will improve the efficiency and minimize the costs of the characterization program.

A. CHARACTERIZATION PROGRAM

The comprehensive characterization program for the oxide-metal composites is outlined in the following steps:

1. Information on fiber cross sections, fiber geometries in the oxide matrix, and metal fiber-to-oxide matrix volume and weight ratios will be collected using polished samples examined in the SEM at low viewing angles ($<10^{\circ}$) and magnifications between 500 to 10,000X. Apart from the usually used emissive mode of operation, reflected electrons will be used at magnifications of 100 to 500X for the examination of the macrostructure within the various growth regions. Semiquantitative chemical analysis will be made with the energy-dispersive detector in the SEM. (Detailed procedures using this analytical technique will be worked out in the future.)

2. Mutual oxide-metal orientation relationships and lattice parameters will be determined using x-ray techniques. Orientation relationships will be studied across the overall composite area to determine preferred growth directions. Oxide-metal-solubilities will be inferred from lattice parameter measurements. These analyses will be carried out using mechanically polished samples.

3. Following suitable chemical etching to expose the metallic fibers, the samples studied under (1) and (2) above will again be examined in the SEM (using primarily stereomicrographs) to

analyze the shapes and forms of the metal fibers. These results will be correlated with the orientation data, growth conditions and etching methods.

4. In selected samples electron diffraction techniques and conventional and high voltage electron microscopy will also be utilized for specific characterization purposes.

Work with existing UO_2-W specimens was performed along the lines of this characterization program, and the initial results are reported.

B. EXPERIMENTAL RESULTS

1. Composite Structures

During the examination of the UO_2-W samples two basically different types of oxide-metal structures have been observed.* The first type is shown in Figure 1 and is characterized by the growth of W fibers essentially uniformly distributed across the melted zone. This growth pattern is interrupted by grain (cell or colony) boundaries where major changes in oxide and metal orientation occur. The second growth type is shown in Figure 2 and has circular areas of the oxide bounded by the composite

*UO_2-W composite samples analyzed in this and subsequent sections of this report were grown both in the School of Ceramic Engineering at Georgia Tech and by the Metals and Ceramics Division of the Oak Ridge National Laboratory.

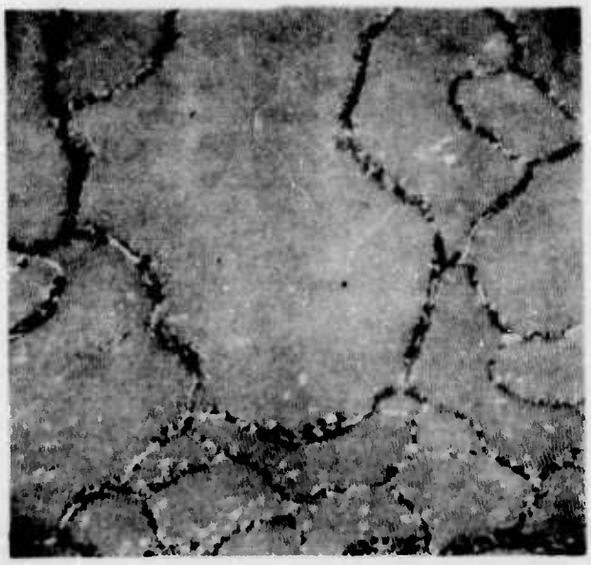

Figure 1. Scanning Electron Micrograph of UO_2-W Composite Displaying Uniform W Fiber Distribution, Emissive Mode of SEM. X100.

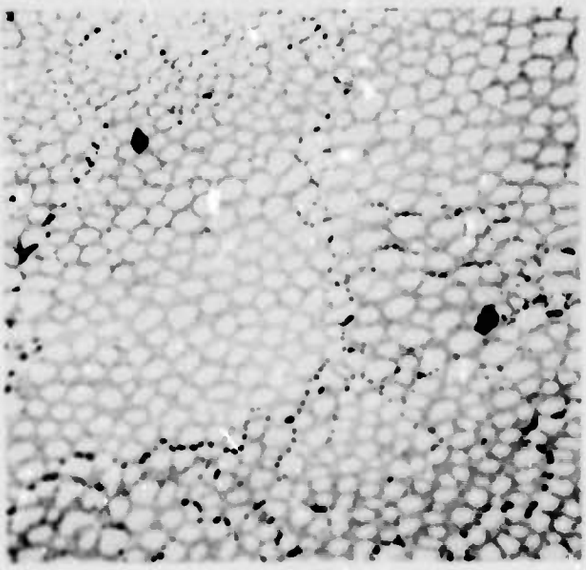

Figure 2. Scanning Electron Micrograph of UO_2-W Composite Displaying Circular Primary Phase Areas of UO_2 plus Eutectic Growth. Reflective Mode of SEM. X100.

(oxide-metal eutectic) structure. The larger grain or cell structure shown in the previous figures is also present in this type of sample. An analysis of the parameters responsible for these different types of growth is presented in Section V of this report.

In the case of the uniform fiber growth, Figure 1, no conclusion can be drawn at present as to the existence of a relationship between grain size, shape and orientation. The shapes of the grains are highly irregular, and the diameters vary from a few microns to a few millimeters. It is noteworthy that no fiber growth occurred in the immediate neighborhood of the grain boundaries. In the structures containing the circular oxide areas, (Figure 2) the location of the grain (cell) boundaries appears to be random, although they traverse the composite region more often than not.

2. Fiber Forms

The observed tungsten fiber shapes certainly depend upon orientation and composite growth conditions, and also often on the chemical etching used to remove a layer of the oxide to expose the fibers for SEM analysis. A variety of cross sections including round, hexagonal, square and rectangular were observed. During etching, the fibers were occasionally altered in such a way that no characteristic crystallographic growth forms were discernible. An example of this behavior is shown

in Figure 3, where etching appeared to alter the fiber shape to a geometry desirable for emitter applications.

Analysis of the various fiber growth forms and conditions leading to their respective growth is in progress. For example, it is difficult to understand hexagonal fiber cross sections in the case of a body-centered cubic material (b.c.c.), such as tungsten. The equilibrium growth form of a b.c.c. material is the rhombo-dodecahedron[5]. When this crystal model, which is surrounded by $\{110\}$ planes only, is cut into two equal halves parallel to any of the opposing pairs of $\{110\}$ planes, a hexagonal cross section is obtained with four equal length edges. The remaining two opposite edges may be longer or shorter than the four equal edges (depending on the particular growth form which has developed). Figure 4 is a transmission electron micrograph* of a UO_2-W composite showing the cross section of several W fibers that comply with the preceeding analysis. Thus hexagonal fiber cross sections indicate $[110]$ as the fiber axis and growth direction.

The role chemical etching plays in altering fiber geometries is under investigation. Figure 5 shows a high magnification view of a single tungsten fiber displaying an octagonal cross section. During etching the fiber morphology was changed by the different etching rates among different crystallographic

*This micrograph was taken by C. S. Yust of the Metals and Ceramics Division, Oak Ridge National Laboratory, Oak Ridge, Tennessee.

Figure 3. Scanning Electron Micrograph of Sharpened Tungsten Fiber Tips After Chemical Etching. Emissive Mode of SEM. X6,500.

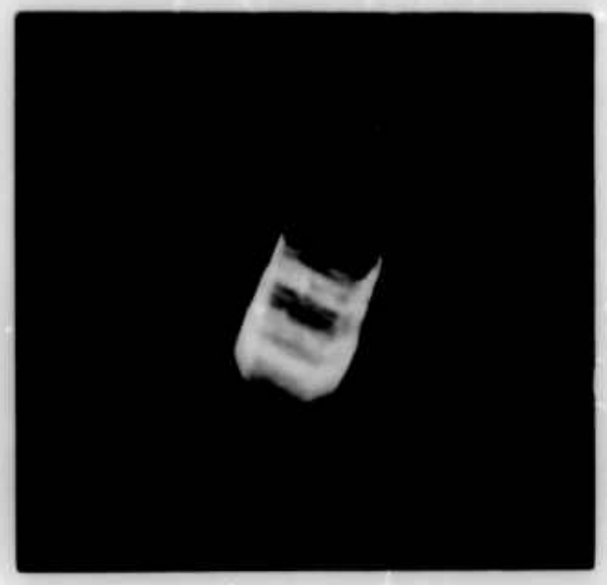

Figure 5. Scanning Electron Micrograph of Single W Fiber. Chemical Etch Has Altered Octagonal Cross Section at Fiber Base to a Square Shape at the tip. Emissive Mode of SEM. X22,000

directions to produce an almost square section at the fiber tip. This growth mode indicates [001] as the fiber axis and growth direction.

3. High Voltage Electron Microscopy (HVEM)

A UO_2-W sample was ion-etched for 154 hours to thin the material for examination in the HVEM.* The tungsten fiber was viewed at approximately 45° off the fiber axis (Figure 6). The fibers were surrounded, as was anticipated, by a pile-up of dislocations. In some cases these dislocations seemed to originate in the fiber and then continue into the oxide matrix. It is noteworthy that no cracks are visible at the fiber-matrix interface, suggesting excellent bonding.

4. X-ray Information

Lattice constant determinations were carried out with numerous UO_2-W samples. The lattice constant measured for tungsten was 3.1649 ± 0.0006 Å; for UO_2 it was 5.4710 ± 0.0007 Å. These values are close to the accepted values for the pure materials, and indicate very little mutual solid solubility between W and UO_2. This result was confirmed on a preliminary basis by nondispersive x-ray analysis in the SEM, although the limit of detection using this technique is unknown at present. No W was

*This work was done at the 1 Mev HVEM facility at U. S. Steel Corporation in Monroeville, Pa. The authors wish to acknowledge the generous help given them by Dr. R. M. Fisher and his staff.

Figure 6. High Voltage Transmission Electron Micrograph of Tungsten Fiber in UO$_2$ Matrix After Sample Thinning by Ion Etching. Fiber Is Viewed at Approximately 45° Off Fiber Axis. X50,000

found in the UO_2 matrix and no U was detected in the W fibers.

Orientation relationships in composite samples were determined with a single crystal orienter (goniostat) possessing several mutually perpendicular and movable rotation axes. All of the samples which were studied contained the grain structure shown in Figures 1 and 2. A great number of orientation relationships are therefore possible; however, preliminary x-ray studies suggest two orientation relationships occurred most frequently in the larger grains. These were $(001)_W \parallel (111)_{UO_2}$ with $[100]_W \parallel [1\bar{1}0]_{UO_2}$ and $(110)_W \parallel (111)_{UO_2}$ with $[1\bar{1}0]_W \parallel [\bar{1}10]_{UO_2}$. Studies are in progress to systematically map the oxide-metal orientation relationships across the composite areas in selected samples.

SECTION IV

THEORETICAL ANALYSIS OF ELECTRON EMITTING ARRAYS

Field emission of electrons from an isolated metallic pin into vacuum has been extensively studied, and excellent reviews are available.[6-9] Graphs and tables are given in these references for the purpose of computing the current density of one tip as a function of applied electric field, work function, and temperature. When a large number of pins are grouped together to form a two-dimensional array, the emission capability is increased, but not as much as is naively expected from simple multiplication of emission-per-pin times the number of pins. Certain theoretical aspects of field emission from such an array are given below, and some numerical results are graphed.

The relevant equation relating the macroscopic field emission current density J to the actual electric field F at the emitter tip of radius r for a square array of side a is given by

$$J = f(\pi r^2/a^2)BF^2 \exp -F_o/F. \qquad (1)$$

The notations used in this report are presented in Table IV. This equation is simply derived by assuming that the effective emitting area is πr^2, that the density of pins per square centimeter is a^{-2}, and that all other corrections are included in f(see below). The presence of a very dense array causes F to

TABLE IV

FIELD EMITTER ARRAY NOTATION

f = correction factor

J = macroscopic current density (amps/cm^2 array area)

ϕ = work function

$f(y)$ = image force barrier lowering term (see ref. 6)

$B = 1.54 \times 10^{-6}/\phi$ (amps/volt^2)

$F_0 = 6.83 \times 10^7 \phi^{3/2} f(y)$ (volts/cm)

F = electric field at emitter tip (volts/cm)

V = voltage (volts)

k = field reduction factor

L = cathode-anode spacing (cm)

a = interpin spacing (cm)

r = pin tip radius (cm)

reduce according to the law:

$$F = V/kr, \qquad (2)$$

where

$$k = \left(1 + \frac{4\pi Lr}{a^2}\right). \qquad (3)$$

The dependence of k on L, r, and a was derived by superposing a one-dimensional potential and a square array of coulomb potentials, and by matching the boundary conditions at each pin tip[10,11]. The effect of pin height was not considered, so the value of k given in equation (3) is probably a lower limit. Clearly it is desirable for k to be as small as possible, $1 < k < 2$, so that excessive voltages need not be applied. A plot of $\log_{10} J$ vs F, as taken from the tables of ref.6, is drawn in Figure 7, assuming that $f = 1$, and $\phi = 4.3$ ev which may be applicable to tungsten with a monolayer of oxygen[6]. Curves in Figure 7 are labelled by the ratios $\pi r^2/a^2 = 1, 10^{-2}, 10^{-4}, 10^{-6}, 10^{-8}$, and 10^{-10}. Thus, Figure 7 and Equations (1)-(3) may be used to compute J given V, r, a, and L. The curves are terminated after a field of $F = 9 \times 10^7$ v/cm is reached. A theoretical analysis of the maximum allowable temperature rise T_m at the tip of a cylinder emitter due to Joule heating shows that the maximum microscopic current density is

$$J_m = 0.24 \times 10^3 T_m^{\frac{1}{2}} h^{-1}. \qquad (4)$$

For $T_m = 1000°K$ and $r = 50 \times 10^{-4}$ cm, this gives $J_m = 1.5 \times 10^6$ amps/cm^2, which corresponds[5] to $F = 9 \times 10^7$ v/cm. Beyond this value of F, destructive cathode heating may result. A replot of Figure 7 is given in Figure 8, where the effect of varying a is explicitly shown with the help of Equations (2) and (3). Values kept constant in this figure are $L = 10^{-2}$ cm. and $r = 0.5 \times 10^{-4}$ cm. Lower voltages are obtained for the curve labelled a = 97Å (one Å = 10^{-8} cm). For values of a chosen smaller or larger than this, the voltage increases to get the same current. If the optimum value of a is desired, it can be computed analytically from

$$a_{optimum} = (4\pi F_o L r^2/V)^{\frac{1}{2}}. \qquad (5)$$

At this optimum, J approximately equals 0.37x (emission per isolated pin)x(density of pins).

One way to subject an observed J-V characteristic to theoretical analysis is to plot it as $\log_{10} J/V^2$ vs $1000/V$. A straight line is expected, whose intercept a_1 and slope a_2 are computed from equations (1)-(3) as

$$\log_{10} J/V^2 = a_1 - a_2 (1000/V). \qquad (6)$$

$$a_1 = \log_{10} (r^2 B/k^2 a^2). \qquad (7)$$

$$a_2 = 0.434\, F_o kr. \qquad (8)$$

This procedure yields Fowler-Nordheim plots. From a_2, the

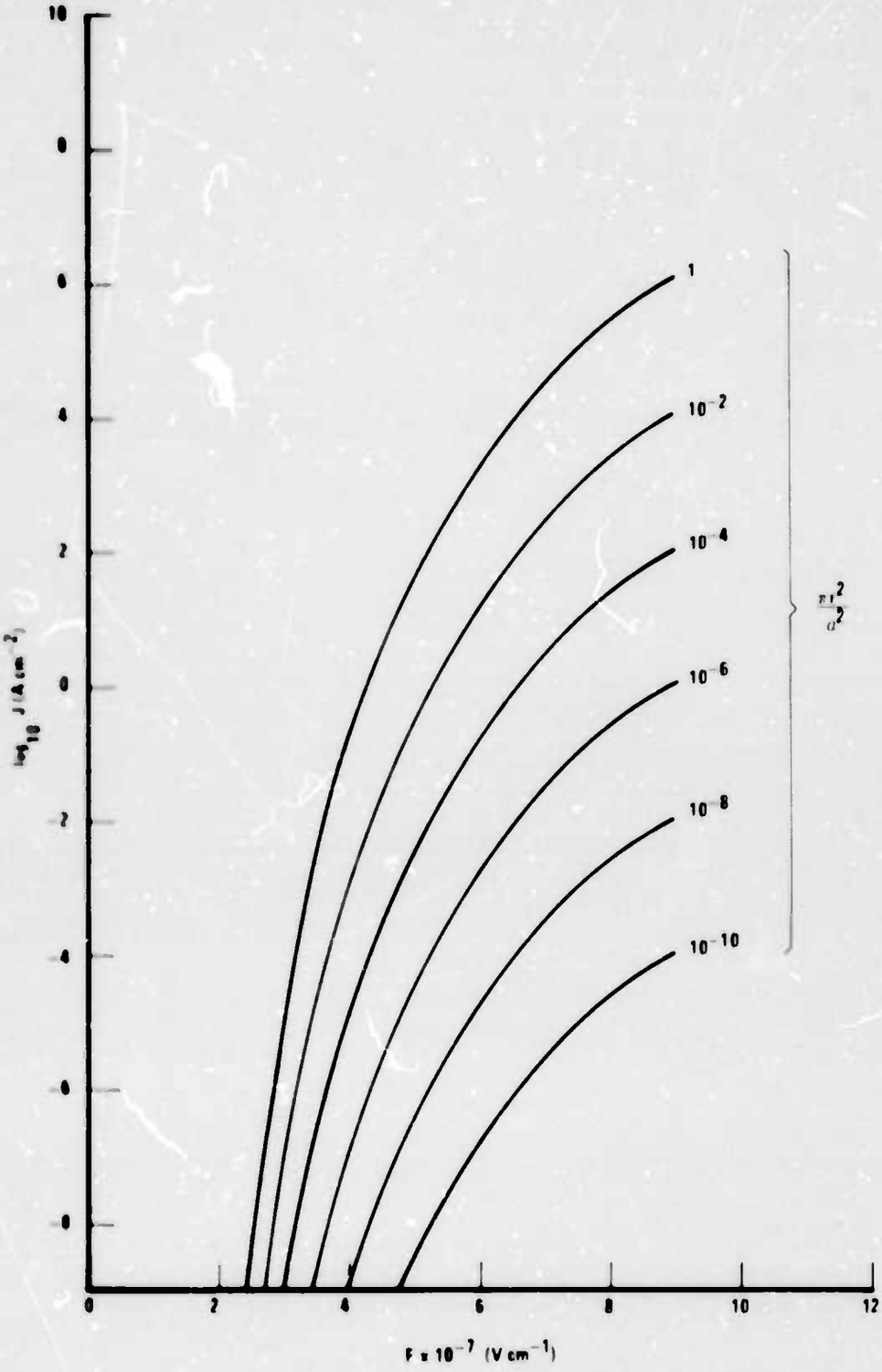

Figure 7. Dependence of Current Density on Electric Field for Various Values of ($\pi r^2/a^2$). In This Plot It Is Assumed That f = 1.

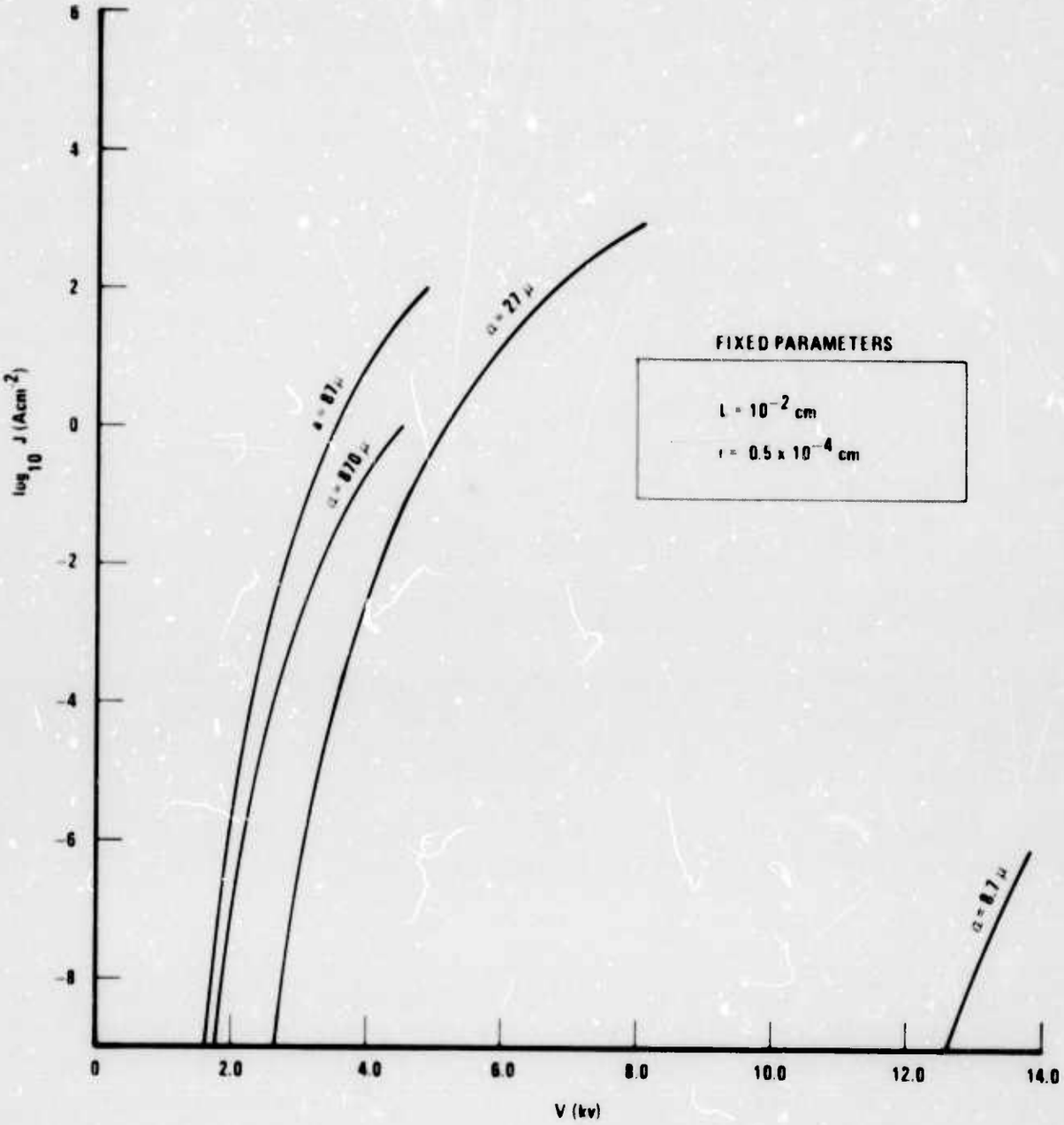

Figure 3. Dependence of Current Density on Voltage, for Various Values of a. Fixed Parameters Are f = 1, L = 10^{-2}cm, and r = 0.5×10^{-4}cm.

product kr can be inferred; and from a_1, it is possible to compute k, if f is known. Typically, $B = 0.3 \times 10^{-6}$ amps/volt^2 and $F_0 \cong 6.5 \times 10^7$ v/cm (for $\phi = 5.7$ ev). In actuality, f may be considerably less than unity for a variety of reasons, so it can be written as

$$f = f_{area} \times f_{polar} \times f_{distribution} \qquad (9)$$

If the tip has appreciable emission from only certain facets, then the fractional emitting area is less than unity and $f_{area} < 1$. If there is a monolayer of adsorbate, then polarization effects cause the barrier height to increase, and theoretical calculations have been made[7,12] which show that

$$f_{polar} = \exp - GN, \qquad (10)$$

where G depends on the polarizability and the effective dielectric constant of the monolayer, and N is the number of adsorbed molecules/cm^2. Experimental results[12] show that one may expect $f_{polar} = 0.05$ for a full monolayer of O_2 on W. $f_{polar} = 0.006$ for a full monolayer of CO on W, and as low as $f_{polar} = 0.5 \times 10^{-4}$ for a fractional monolayer of H_2 on W. Clearly, there is a large penalty to pay for having a monolayer of adsorbate present on the surface of a field emitter tip. The influence of different pin shapes, mainly distribution of pin diameters, f distribution, in the field emission performance is under investigation and will be described in a subsequent report.

SECTION V

FORMATION OF OPTIMUM EMITTING ARRAYS

The major objective of this portion of the research project is to study growth in a model oxide-metal system, i.e. UO_2-W, and establish the role controllable growth parameters exert on the composite microstructures. As the project progresses, emphasis will be placed on those variables which produce structures which will yield optimum electron emission performance. A prototype composite growth facility has been constructed. Existing microstructures have been analyzed on the basis of oxide-metal ratios, the phase diagram, and variable growth rates to gain understanding about the growth process in oxide-metal systems. After growth the composites have been chemically treated to expose the tungsten fibers (primarily for electron emission testing), and the etching procedures are described. Several attempts have also been made to electrolytically sharpen the tips of the tungsten fibers for enhanced emission.

A. COMPOSITE GROWTH EQUIPMENT

A schematic diagram of the prototype facility used for the oxide and oxide-metal composite growth is shown in Figure 9.

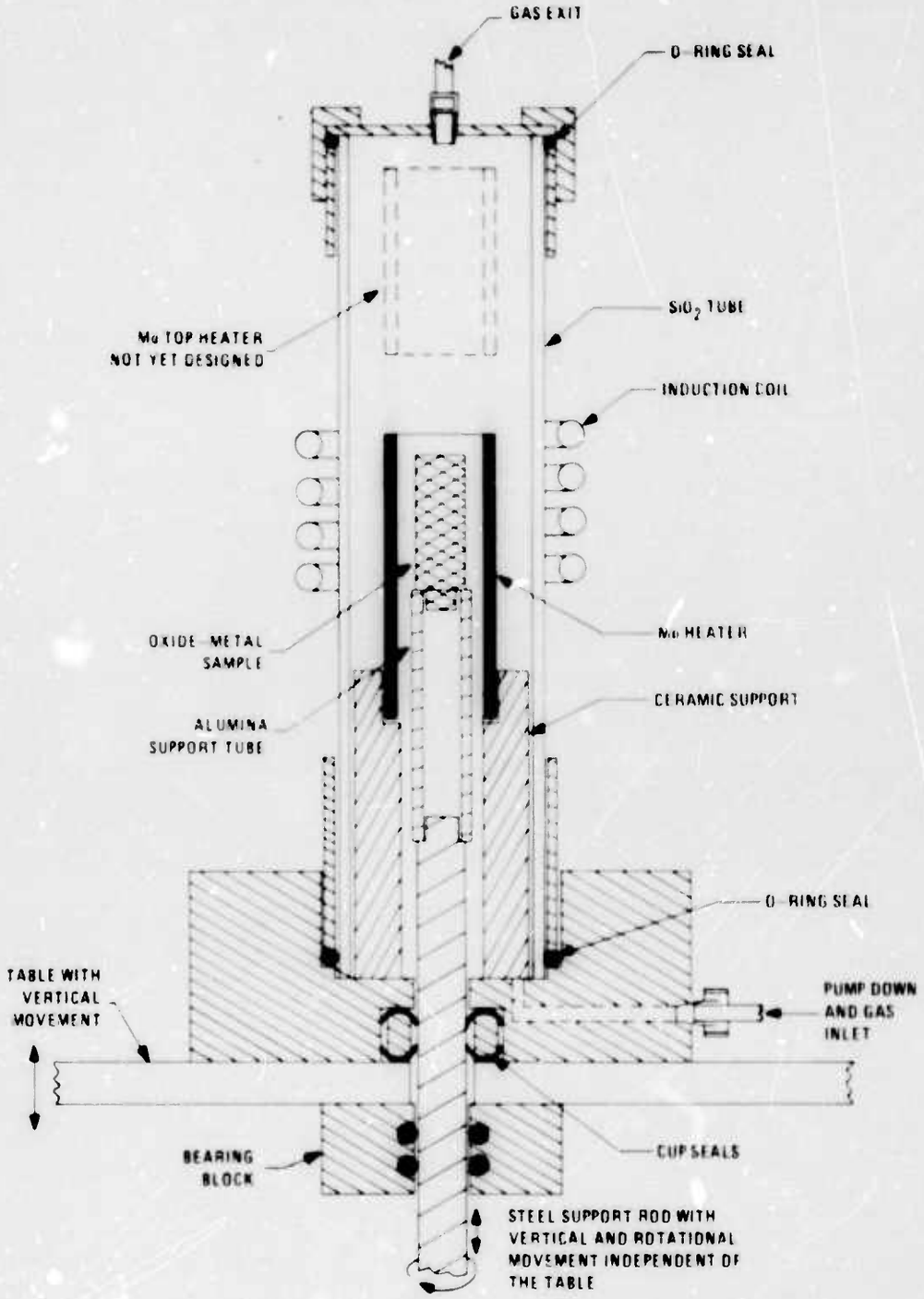

Figure 9. Schematic Diagram of Facility for the Growth of Oxide-Metal Composites.

This facility provides both rotation and vertical translation of the sample, and variable positioning of the molybdenum heaters. The system may be evacuated as well as operated in controlled atmospheres, usually nitrogen or nitrogen-hydrogen mixtures. The prototype facility is currently operative, although the design and construction of the top molybdenum preheater is incomplete. One improvement in this growth facility is the use of a hydraulic system to raise and lower the sample. The use of a hydraulic cylinder, rather than some type of mechanical drive normally incorporated in systems of this type, should minimize fluctuations in growth rates and provide a more stable liquid-solid solidification front. The small volume of the growth chamber enables rapid changes in atmosphere for stoichiometry control; preliminary testing indicates that the oxygen and/or water vapor content in the system is low enough to keep the oxidation of the refractory metals to an acceptable level. The location of the rf coil outside the silica tube minimizes arcing and the problems associated with getting a satisfactory high frequency rf lead-through into a closed system. One drawback of the external work coil is the inability to achieve close sample-coil spacing to improve coupling; however, initial testing of UO_2 and UO_2-W mixtures using a frequency of 4.6 mhz indicated these materials could be easily melted with the present design.

B. ANALYSIS OF OXIDE-METAL SOLIDIFICATION

Since the first growth of the UO_2-W composites[1], there has been no published information on the factors controlling the type of structures obtained during unidirectional solidification of oxide-metal mixtures. The structures of available UO_2-W samples and the initial UO_2-W composites grown on this project have been analyzed, and a preliminary interpretation of the growth parameters operative during this high temperature solidification process is presented.

Since there is no existing phase diagram for the system UO_2-W, a tentative diagram is proposed in Figure 10 which is consistent with a number of experimental observations. The UO_2-W solidification behavior indicated these components form a eutectic system. Very limited solid solubility is proposed because x-ray information showed lattice parameters very close to the standard values for pure UO_2 and W. The eutectic temperature cannot be more than two or three hundred degrees below the melting point of UO_2, because melting pure UO_2 or UO_2-W mixtures yielded very similar sample surface temperatures. Several preliminary experiments performed at the Oak Ridge National Laboratory* have explored melting UO_2 crystals on a tungsten ribbon filament. The reaction (eutectic temperature) between the oxide and metal occurred at $2640^\circ \pm 30^\circ$C. The eutectic composition is estimated.

*Personal communication, Benjamin Oliver, consultant to the Metals and Ceramics Division, Oak Ridge National Laboratory, Oak Ridge, Tennessee.

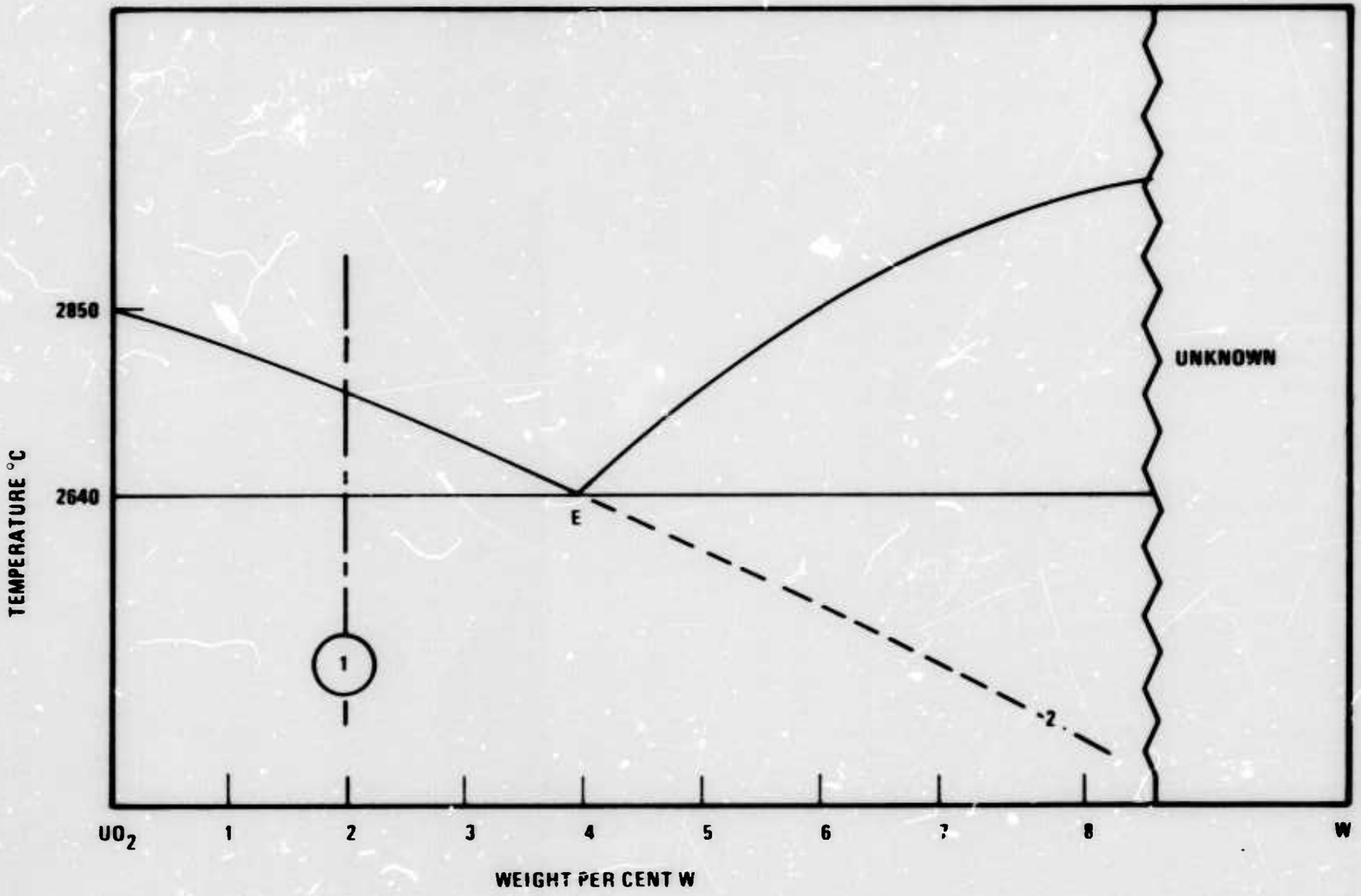

Figure 10. Proposed Phase Diagram for the System UO_2-W.

from analysis of SEM pictures, to occur between 3 to 5 weight percent tungsten.

Initially it should be pointed out that simply using the starting oxide-metal ratio for the composition in the UO_2-W phase diagram is inaccurate, because transport processes are very rapid at the extremely high temperatures needed to melt these mixtures; and significant quantities of the metal are lost from the molten zone, probably by vaporization or a diffusion mechanism. Two basic types of oxide-metal composite structures have been observed to date. Figures 11a and 11b show a sample containing the tungsten fibers uniformly embedded in the UO_2 matrix across the entire melt area. Figures 11c and 11d are typical structures obtained from melting noneutectic oxide-rich mixtures. These samples exhibit rather uniform circular areas of primary oxide phase separated by a continuous zone of the eutectic structure. (Lower magnification views of these two different types of structures are also shown in Figures 1 and 2 in this report.) Pertinent growth and structure information for the samples shown in Figure 11 are given in Table V. The W fiber diameter, density and eutectic composition are average values obtained by examining scanning electron micrographs of many growth regions in these and other similar samples. The eutectic composition was determined by a simple area count of tungsten fibers and converting this information to weight percent metal using theoretical density values for the UO_2 and tungsten.

Figure 11. Scanning Electron Micrographs of UO_2-W Composites Showing Influence of Oxide-Metal Ratio and Growth Rate on the Composite Structure and W Fiber Diameter and Density. Samples Chemically Etched to Expose the Fibers. Emission Mode of SEM.

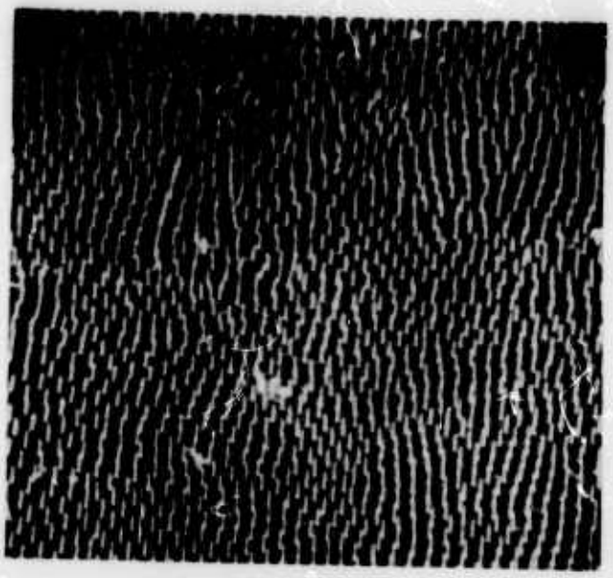

(a) Near Eutectic Composition, Slow Growth Rate, X500.

(b) Near Eutectic Composition, Fast Growth Rate, X500.

Figure 11 (cont.)

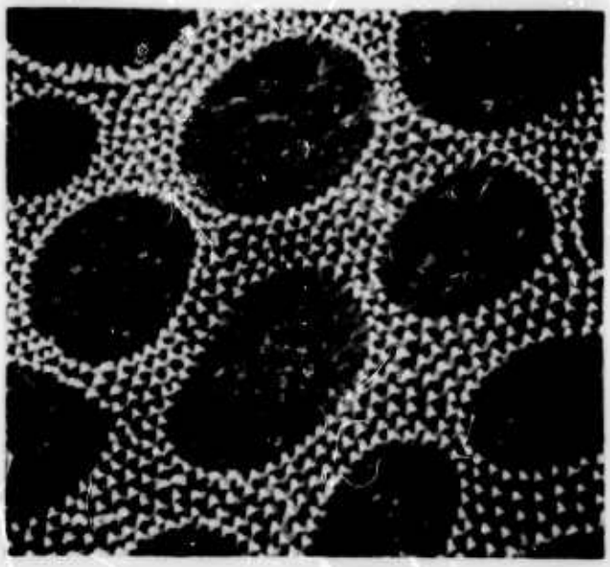

(c) Oxide-Rich Composition. Slow Growth Rate. X700.

(d) Oxide-Rich Composition. Fast Growth Rate. X700.

TABLE V

GROWTH AND STRUCTURAL INFORMATION FOR UO_2-W COMPOSITES SHOWN IN FIGURE 11

	(a)	(b)	(c)	(d)
Starting Composition Weight % W	12.5	10	10	5
Growth Rate mm per hr	15	50	15	60
Fiber Diameter microns	0.75-0.94	0.33	0.90	0.42
Fiber Density (eutectic areas only) $x10^{-6}$ per cm^2	4.5	25	6.5	56
Eutectic Composition Weight % W	3.6-5.3	3.8	7.1	12.8

The following analysis of the UO_2-W solidification behavior is proposed to explain these different composite structures. Examination of many areas in samples displaying uniform growth, Figure 11a and 11b, indicated that the eutectic composition in the System UO_2-W occurred between 3.6 and 5.3 weight percent W. This analysis is the justification for the eutectic location shown in the proposed phase diagram drawn in Figure 10. Similar examinations of only the eutectic areas in the samples containing the circular primary areas of UO_2 indicated a eutectic composition between 7.1 to 12.8 weight percent W. An explanation for this apparent discrepancy follows the analysis of Lundquist et.al.[13] They showed that solidifying near eutectic compositions in metal-metal systems produced fine "eutectic" structures, whereas solidifying off-eutectic mixtures lead to primary phase regions distributed throughout the eutectic structure.

During the cooling of oxide-rich UO_2-W mixtures, represented in general by composition 1 in the phase diagram, the primary phase nucleated at a temperature higher than the eutectic temperature; and, as cooling proceeded, the composition of the remaining liquid moved down the liquidus line toward the eutectic composition. Some undercooling is expected and the liquid follows the metastable extension of the liquidus curve from E towards 2 and became richer in tungsten. When sufficient undercooling was available to initiate nucleation, the tungsten content of the liquid approached 7 to 12 weight percent. Thus,

supercooling can account for the higher W concentration (7 to 12%), in the eutectic areas of samples (Figure 11c and 11d) containing the primary UO_2 regions. Also, it is noteworthy that increasing the growth rate should increase the undercooling and, hence, the amount of W in the eutectic areas of the faster grown samples. This behavior was observed for samples (c) and (d) (Table V). Since the melting point of UO_2 and the proposed eutectic temperature have a small temperature spread, the liquidus line has a comparatively small slope, and the amount of undercooling required to change the metal-oxide ratios from 4 to 8-10% tungsten would be only 200 to 400°C; not unreasonable values considering the extremely high eutectic temperature in this system.

The influence growth rate had on the fiber density and diameter can be readily seen by comparing the structures shown in Figures 11 and the data in Table V. The slower grown samples produced large, widely spaced fibers; whereas increasing the growth rate decreased fiber size and spacing. This behavior is typical of the eutectic solidification found in metal-metal systems, although the structures are usually lamellar rather than the fiber or rod type.

Occasionally in some areas of oxide-rich samples (Figure 11c and 11d) walls of tungsten were found partially encircling the primary UO_2 regions. A typical structure is shown in Figure 12. Similar behavior has been seen in all metal systems by

Figure 12. Scanning Electron Micrograph of Oxide-Rich UO_2-W Structures Showing W "Halo" Partially Encircling Primary Phase Areas of UO_2. Emission Mode of SEM.

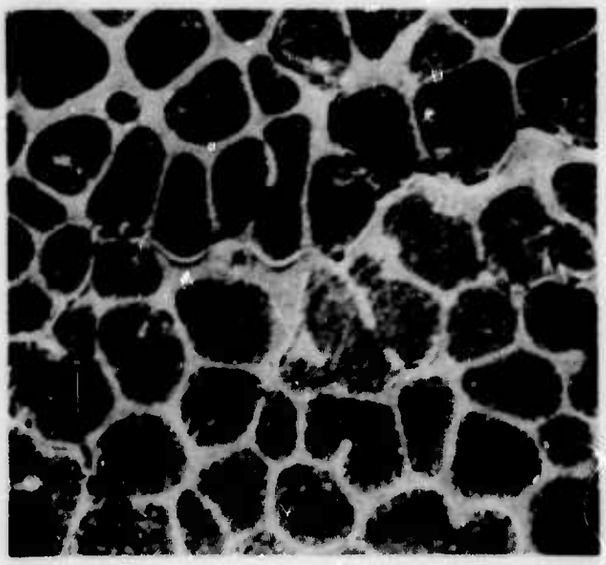

(a) X300.

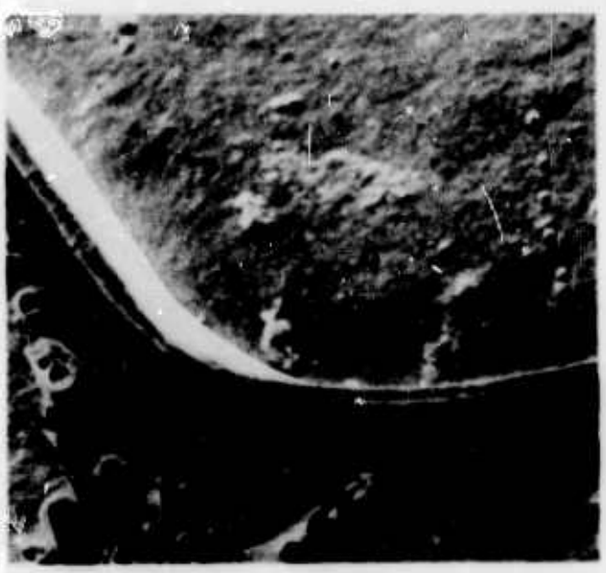

(b) X1,500.

Lundquist et.al.[13], and they labeled this occurrence the formation of "halos". These authors postulated that if extensive supercooling and supersaturation of the liquid occurred, the excess phase (W in this case) must be removed prior to the simultaneous precipitation of both phases from the "eutectic" liquid.

The analysis and controlled growth of a variety of UO_2-W mixtures is continuing. The initial attempts to melt tungsten-rich mixtures using the induction heating technique have been unsuccessful, for reasons not clear at present.

C. CHEMICAL ETCHING PROCEDURE

The UO_2-W composites used both for emission testing and structure analysis in the SEM were chemically etched to remove an oxide layer and expose the tungsten fibers. (All of the scanning electron micrographs shown in the preceeding figures were of etched samples.) This etching technique will be briefly described along with some preliminary electrolytic work designed to sharpen the tips of the fibers for better field emission performance.

For chemical etching the UO_2-W composite samples were first mechanically polished to a bright finish using successively finer grinding paper and finishing with one micron diamond paste on a nylon cloth. Reflected light examination was used to check the surface prior to chemical etching. An etching solution was

prepared consisting of[14]:

(1) 20 ml saturated chromic acid

(2) 10 ml glacial acetic acid

(3) 7 ml concentrated nitric acid

(4) 5 ml 48% hydrofluoric acid

Polished samples usually in the shape of wafers were clipped to a shaft rotating at several revolutions per second and immersed in the etching solution for a predetermined time, depending on the fiber length desired. After etching the samples were removed from the etchant and washed by rotation in a water bath for twenty minutes. Heights of the exposed fibers were determined from scanning electron stereomicrographs of differently etched samples. This information will be given in the next report, as the present results are widely scattered and appear unreliable.

Electrolytic etching techniques are widely used to produce very small diameter tungsten tips starting with tungsten wires. These techniques usually employ an alkali hydroxide solution as the electrolyte. Preliminary attempts to adapt this scheme to sharpen the W fibers in chemically etched UO_2-W samples were unsuccessful, as the hydroxide solutions severely attached both the fibers and matrix. Some promising results were obtained

using a dilute Na_2CO_3 electrolytic etching solution with the UO_2-W composites, and further work in this area is planned.

SECTION VI

ELECTRON EMISSION MEASUREMENTS

An important facet of this research program is the systematic study of the high field emission characteristics of melt-grown oxide-metal composites. The experimental apparatus incorporates a diode with adjustable interelectrode spacing mounted within an ultrahigh vacuum chamber. Construction is such as to permit the application of high interelectrode potentials. Measurement instrumentation consists of conventional electrometers, recorders, and power supplies. Principal efforts during the period covered by this report have been directed toward facility development. Some limited experimental emission measurements have established the feasibility of the experimental method and have confirmed the satisfactory operation of the apparatus.

A. EXPERIMENTAL FACILITY

The vacuum enclosure illustrated in Figure 13 is an all stainless steel bakeable "cross" chamber. Most of the vacuum seals are metal o-ring compression seals using soft aluminum wire; the flange around the high voltage feedthrough is a Varian "Conflat" flange. The pumping system consists of a four-inch

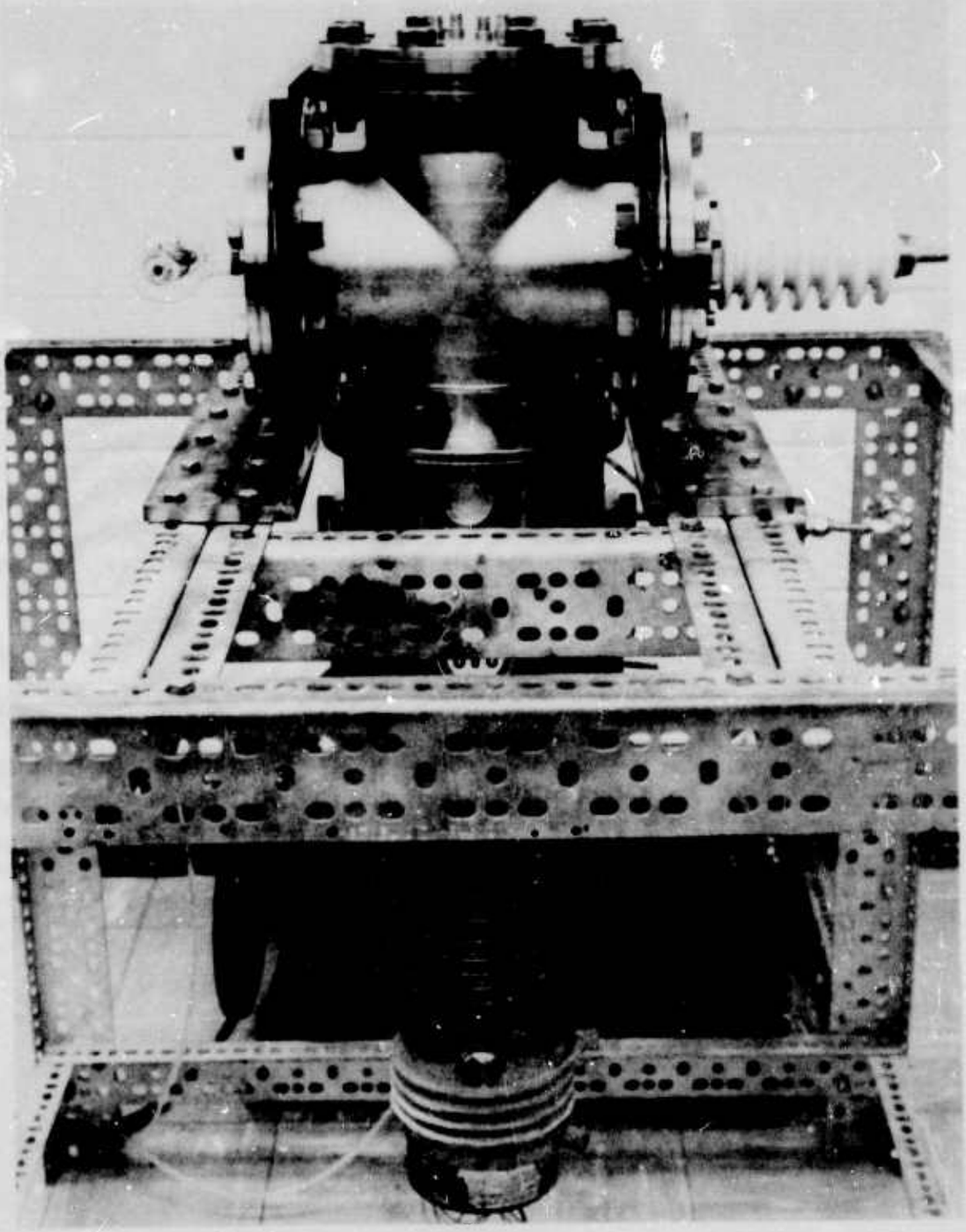

Figure 13. Overall View of Electron Emission Test Facility and Associated Vacuum Equipment.

oil diffusion pump, a water cooled chevron baffle, a freon cooled baffle, a mechanical pump and associated pumping and bakeout controls. A base pressure of the order of 1×10^{-8} torr is attainable without bakeout. All feedthroughs, with the exception of the high voltage feedthrough, are of the coaxial type permitting shielding of all instrumentation leads.

The assembled diode structure is shown in Figure 14. The molybdenum anode and cathode structures have variable axial spacing. All insulators are steatite or alumina. The polished and etched oxide-metal composite emitter is mounted on the cathode rod with silver paste. A negative potential is applied to the emitter and the current collected by the anode is measured with an electrometer and a strip-chart recorder. A protective series resistor is included in the circuit to prevent damage to the electrometer and the sample should a short circuit between the emitter and collector inadvertently occur.

B. PRELIMINARY FIELD EMISSION RESULTS

Preliminary data have been obtained from a single UO_2-W composite employing a sample-to-anode spacing of approximately 0.010 inch. With this spacing, a current density of greater than 10^{-8} amp/cm^2 was measured with an applied potential of 800 V, and a current density of greater than 10^{-4} amp/cm^2 was observed with an applied voltage of 2300 V. Reversing the potential applied to the test diode conclusively showed that the current

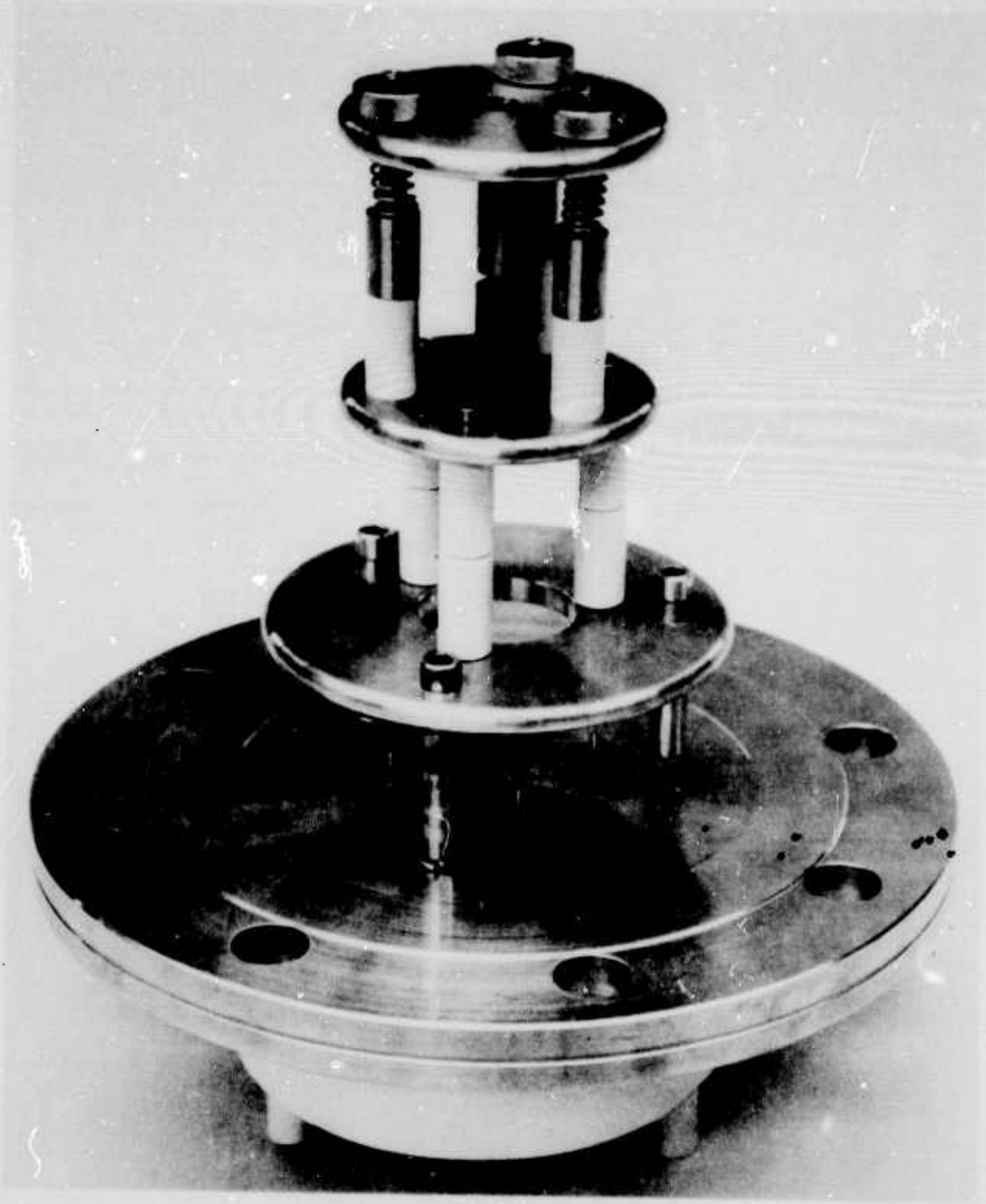

Figure 14. Assembled Diode Structure for Emission Testing.

was due to true electron emission. The short term stability of the emission appeared to be poor; fluctuations of $\pm$20 percent were not uncommon.

These short term fluctuations could conceivably be due to some type of gaseous breakdown within the test diode or to some dynamic process involving the transfer of emission from different groups of pins. It is anticipated that the lower pressure attainable with system bakeout (estimated to be less than 10^{-9} torr) will greatly reduce any breakdown effects and thus facilitate a determination of the cause of the unstable current.

In spite of the apparently poor short term stability, the average current as monitored with a recorder did not change by more than a few percent over a period of approximately 24 hours. Also, within reasonable limits, the average current measurements were reproducible over the test period of approximately one week. However, it was noted that there appeared to be an increase in the emitted current with time. The cause of this apparent increase is unknown and is being investigated.

SECTION VII

SUMMARY

During the last six months work has been underway on ARPA Order No. 1637 for the development of melt-grown oxide-metal composites containing between 4 and 25 million less than 1μ diameter tungsten fibers per square centimeter, uniformly embedded in an oxide matrix, and the evaluation of these materials for electron emission applications. The research program is divided into five areas to meet the project objectives:

(1) Unidirectional Solidification Behavior of Oxide-Metal Systems.

(2) Structural and Chemical Characterization of Oxide-Metal Composites.

(3) Theoretical Analysis of Electron Emitting Arrays.

(4) Formation of Optimum-Emitting Arrays.

(5) Electron Emission Measurements.

A number of oxides, oxide compounds and oxide mixtures have been tested to determine their suitability for induction melting using high frequency rf heating. Only ZrO_2 (CaO or Y_2O_3 stabilized), ZnO, CdO, NiO, Cr_2O_3, TiO_2, CeO_2, $ZnO \cdot TiO_2$, $ZnO \cdot Al_2O_3$, $BaTiO_3$ and mixtures of NiO-MgO and Al_2O_3-NiO were melted from the many materials tested; and, of this list, only the stabilized ZrO_2 and CeO_2 established stable enough molten

geometries to warrant further study with metal additions. An analysis of some of the difficulties encountered melting oxide materials with rf heating and future approaches designed to increase the list of materials which may be induction heated are presented.

Techniques and procedures which provide adequate characterization of oxide-metal composites and the structural and chemical information necessary to interpret and predict the solidification behavior in oxide-metal systems are being developed in three areas: Scanning electron microscopy (SEM), energy dispersive analysis, and x-ray diffraction. Scanning electron micrographs have been used to analyze the various oxide-metal structures and the growth modes of individual tungsten fibers. Several fiber shapes have been related to growth directions. Preliminary x-ray data indicated that two oxide-metal orientation relationships are dominant in UO_2-W composites.

A theoretical field emission model has been developed to provide an insight as to the field distribution in the vicinity of a periodic array of emitting pins. This analysis indicates desirable pin spacings for maximum current density and the effect pin diameter and interelectrode spacing will have on the voltage needed to produce different electric fields. Graphs illustrating this information are included.

The growth and analysis of oxide-metal composites has progressed to the point where preliminary interpretation of the

different types of microstructures obtained in the system UO_2-W can be made using starting oxide-metal ratios, a proposed phase diagram, and growth parameters. Typical composite structures obtained during the controlled solidification of UO_2-W mixtures are shown in Figure 11 of this report. The chemical etching technique used to dissolve a layer of the oxide matrix and expose the W fibers for emission testing and analysis in the SEM is described.

A study of the field emission obtainable from oxide-metal composites under ambient temperature conditions has been initiated. A stainless steel ultrahigh vacuum system in conjunction with a diode structure is employed for this testing. Parameters under investigation include diode electrode spacing, field strength, critical current density (that current density at which pin damage occurs), input power, and emitter lifetime. Initial testing of a single suitably etched UO_2-W sample was most encouraging as field emission was readily obtained at a reasonable applied voltage. Reversing the potential applied to the test diode conclusively showed that the current was due to true electron emission. During this first test the current density was low, approximately 10^{-4} amps per cm^2, and erratic; but the average current remained within several percent for a reasonable time period. Emission testing of different oxide-metal geometries is continuing.

REFERENCES

1. A.T. CHAPMAN, et. al., J. Am. Cer. Soc. 53 (1) 60 (1970).

2. M.D. WATSON, et. al., J. Am. Cer. Soc. 53 (2) 112 (1970).

3. D.N. HILL, "Internal Zone Melting of Refractory Oxides Using Induced Eddy-Current Heating," M. S. Thesis, School of Ceramic Engineering, Georgia Institute of Technology, September 1969.

4. A.T. CHAPMAN and G. W. CLARK, J. Am. Cer. Soc. 48 (9) 494 (1965).

5. B. HONIGMANN, Gleichgewichts-Und Wachstumsformen von Kristallen, Steinkopff Verlag, Darmstadt, (1958).

6. W.P. DYKE and W.W. DOLAN, Advances in Electronics and Electron Physics, VIII, Edited by L. Marton, Academic Press, N. Y. (1956).

7. A.G.J. VAN OOSTROM, Philips Research Reports Supplements, No. 1, (1966) pp. 1 - 102.

8. R.H. GOOD and E.W. MULLER, Handbuch der Physik, vol. 21, Springer Publishers, Berlin, (1956).

9. R. GOMER, Field Emission and Field Ionization, Harvard University Press, Cambridge, (1961).

10. J.D. LEVINE, Surface Sci. 10 313 (1968).

11. J.D. LEVINE, (to be published in RCA Review, 1971).

12. D. MENZEL and R. GOMER, J. Chem. Phys. 41 3311, 3329, (1964).

13. B.E. LUNDQUIST, et. al., J. of Metals 91 204 (1962-63).

14. A.J. MANLY, J. Nucl. Mater., 15 143 (1965).

DISTRIBUTION LIST

DISTRIBUTION	NO. OF COPIES
DIRECTOR ADVANCED RESEARCH PROJECTS AGENCY ATTN: PROGRAM MANAGEMENT DR. M. J. SINNOTT WASHINGTON, D.C. 20301	5
COMMANDING GENERAL U.S. ARMY MISSILE COMMAND ATTN: AMSMI-RND REDSTONE ARSENAL, ALABAMA 35809	20
DEFENSE DOCUMENTATION CENTER CAMERON STATION ALEXANDRIA, VIRGINIA 22314	20
COMMANDING GENERAL U.S. ARMY MATERIAL COMMAND ATTN: AMCRD-PT WASHINGTON, D.C. 20315	1